Power Cable Mass Estimation for Electric Aircraft Propulsion

Eliot Aretskin-Hariton[*]
NASA Glenn Research Center, Cleveland, OH, USA

Mark Bell, PE[†]
HX5 LLC, Cleveland, Ohio, USA

Sydney Schnulo[‡], Justin Gray[§]
NASA Glenn Research Center, Cleveland, OH, USA

Electric aircraft propulsion relies on power transmission cables to carry energy through the vehicle's electrical power train. The mass of these cables is an important consideration in overall aircraft empty weight, and hence cable design methods that can offer lower weight cables offer a significant opportunity. This paper compares three strategies for cable design: selection of cables from off-the-shelf options, design based on steady-state thermal limits, and design based on transient thermal limits. The thermal models consider both conductor diameter and insulation thickness, as well as a comparison between multiple conductor materials. The thermal analysis evaluates the transfer of waste heat from the conductor to the insulation and from the insulation to the air via convection. Optimizations to minimize cable mass by changing conductor radius and material properties were performed using all three modeling approaches and the results show that both custom sized cables using both steady-state and transient based model offer potential mass savings.

[*]Aerospace Engineer, Intelligent Control and Autonomy Branch,
[†]Electrical Engineer IV
[‡]Aerospace Engineer, Propulsion Systems Analysis Branch
[§]Aerospace Engineer, Propulsion Systems Analysis Branch

Nomenclature

Acronyms

AWG	American Wire Gauge
COTS	commercial off-the-shelf
EAP	Electrified Aircraft Propulsion
eVTOL	Electric Vertical Takeoff and Landing
IEC	International Electrotechnical Commission
MTO	maximum takeoff weight
PVC	polyvinyl chloride
SVD	Single Void Discharge
UAM	Urban Air Mobility

Variables

α	minimum breakdown voltage of air in the cavity (V)
α_r	scale factor, resistance temperature $(1/C)$
A_c	area, conductor (cm^2)
A_i	area, insulator (cm^2)
A_s	area, sheath (cm^2)
C	low voltage cable insulation thickness adjustment (cm)
C_c	circumference, conductor (cm)
C_i	outer circumference, insulator (cm)
CPc	specific heat, conductor $(J/C/g)$
CPi	specific heat, insulator $(J/C/g)$
$\frac{dT_c}{dt}$	time derivative of T_c (C/s)
$\frac{dT_i}{dt}$	time derivative of T_i (C/s)
ϵ	dielectric permittivity of insulator
h	convective heat transfer coefficient $(W/C/cm^2)$
HC_c	heat capacity per unit length, conductor $(J/C/cm)$
HC_i	heat capacity per unit length, insulator $(J/C/cm)$
I	current, conductor (amp)
k	thermal conductivity, insulator $(W/cm/C)$
K	shape factor of insulation void
$\bar{m}_{tot}$	mass per unit length, total (g/cm)
$\bar{m}_c$	mass per unit length, cable (g/cm)
$\bar{m}_i$	mass per unit length, insulation (g/cm)
$\bar{m}_s$	mass per unit length, sheath (g/cm)
Q_i	heat flux, insulator (W/cm)
Q_c	heat flux, conductor (W/cm)
Q_∞	heat flux, ambient (W/cm)
ρ_i	density, insulator (g/cm^3)
ρ_c	density, conductor (g/cm^3)
ρ_s	density, sheath (g/cm^3)
r_c	radius, conductor (cm)
R_c	resistance, conductor (Ω/m)
R_{ref}	resistance, conductor at reference temperature (Ω/m)
T_c	temperature, conductor (C)
T_{ci}	temperature, conductor and insulator (C)
t_i	thickness, insulation (cm)
T_i	temperature, insulator (C)
t_s	thickness, sheath (cm)
T_∞	temperature, wingbox ambient (C)
T_{ref}	temperature, reference (C)
t_v	thickness of insulation void (cm)
V_{max}	line voltage, maximum (V)

I. Introduction

Modeling Electrified Aircraft Propulsion (EAP) subsystems presents many challenges to traditional design methods and tools, due to new interactions between subsystems that were not present with conventional propulsion. Although EAP subsystems tend to be highly efficient, the waste heat they produce is low temperature and difficult to reject. Hence thermal management becomes a critical sizing consideration for many EAP applications.[1] While thermal considerations have always been a critical governing factor in the size and mass of power cables, for EAP applications the higher level of power being transferred means that cable mass contributes much more significantly to aircraft empty weight. Accordingly, there is a need to incorporate thermally-constrained cable designs into the aircraft mass estimation process and tie that directly to the conceptual system level EAP design.

Previous work by the authors has focused on using gradient-based optimization methods for EAP design that tightly coupled thermal management into the aircraft design process.[2–5] These studies are based on the quadrotor concept vehicles shown in Fig. 1 developed by NASA's Revolutionary Vertical Lift Technologies project.[6,7] The goal of these studies was to expand the capability of optimization software tools, understand how subsystems interact with each other, and explore different ways of modeling subsystems. In prior work, thermal limits for power cables were accounted for in an extremely simple manner by assuming that conductor heat could be moved to the ends of the cables without a mass penalty. The heat was then dissipated by the thermal management system, which was also used to cool the motors.[2] The existing thermal management system was composed of a heat exchanger and fluid pump, which could be increased in size and pumping speed to increase cooling at the expense of mass or power. Those results showed that by changing the conductor material, maximum takeoff weight (MTO) could be decreased by 6%. This factor included the effects of thermal and battery re-sizing to accommodate larger cooling flows. The reduction in MTO was achieved by making the cables lighter at the expense of increasing resistance. Effectively, the optimizer chose to increase power to save weight.

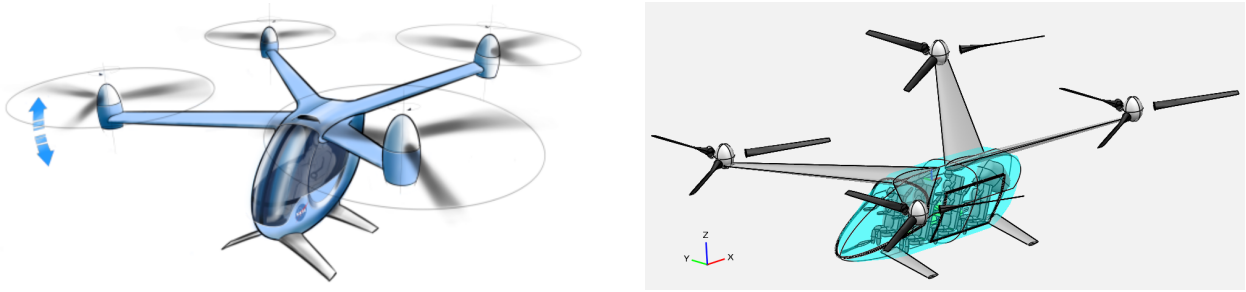

(a) 1-passenger quadrotor

(b) 6-passenger quadrotor

Figure 1: Quadrotor concept vehicles side-by-side.

This work examines three different power cable mass estimation approaches for EAP applications based on a sizing process that considers electrical current requirements, conductor material properties, and thermal limits. The three methods examined are off-the-shelf catalog selection, design based on steady-state thermal limits, and design based on transient thermal limits. It is important to note that while this work compares the three methods on equal footing, it does not consider all of the safety margins outlined by the wiring requirements in the SAE-AS50881 standard for aircraft design.[8] In practice for detailed cable design, additional safety margins and failure analyses could be layered on top of any of the three methods examined in this work. Typical commercial off-the-shelf (COTS) power cables are sized based on terrestrial or marine applications using a steady-state model with assumed maximum current ratings and constant ambient temperatures. SAE-AS50881[8] spells out additional considerations for aircraft applications. The steady-state assumption simplifies the analysis, but as the prior work has shown, EAP systems do not necessarily operate at a steady-state thermal condition, especially for short ranged Electric Vertical Takeoff and Landing (eVTOL) designs. Hence, steady-state sizing practices could drastically oversize the power cables

and add significant empty weight to the aircraft. eVTOL aircraft in particular are very sensitive to component weight which makes any oversizing of the cables expensive in terms of vehicle mass.[3] As an alternative, this paper considers a transient method to design cables based on their performance throughout a reference mission.

Thermal modeling in this work considers waste heat generated by resistance in the power cables that is moved via conduction from the electrical conductor through the cable insulation, and then transferred via convection to ambient air. This thermal model is validated by sizing cables using COTS assumptions and showing that similar cable dimensions and thermal performance are achieved. Next the model is used to propose a more realistic sizing process for aircraft that can yield substantial reductions in power cable mass.

In general, changing component weights for the aircraft requires resizing the vehicle in order to get accurate vehicle level trends. Design of the entire aircraft is out of scope for this work, so a constant MTO assumption is used. This results in a constant power profile during the mission. In order to respect the constant MTO assumption, any decrease in power cable mass is used to increase payload mass. The conductor material is a design variable which the optimizer is allowed to vary to evaluate the change in cable mass. Cable insulation radius is calculated based on the diameter of the conductor and the maximum voltage of the vehicle during the mission using the Single Void Discharge (SVD) method.[9,10] This method was selected because it yields a closed-form solution that matches well with published data. Conductor and insulator temperatures are tracked throughout the mission. These temperatures are regulated by convective heat transfer to ambient air inside the wing box. Prior work assumed power cable waste heat was rejected through a centralized heat exchanger.[3] In this work a passive-cooling approach avoids the consideration of designs that spend power to dissipate heat in the power cables.

All of the models built for this work are created in the OpenMDAO framework.[11] OpenMDAO uses analytic derivatives to perform gradient-based optimization of large solution spaces with thousands of design variables. Time-based calculations of the vehicle trajectory and states are performed using the Dymos library built ontop of OpenMDAO.[12] Dymos uses multispectral methods to model trasient analysis in a manner that is well matched to use in an optimization context A second implementation is planned for the Electrical Modeling and Thermal Analysis Toolbox (EMTAT),[13] which is a Matlab-based software package. The simplicity of the models presented in this paper should allow the reader to easily adapt the presented models to the reader's preferred framework.

The rest of the paper is organized as follows: In Sec II the cable model and optimization problem are described. This has three subsections, Sec II.A covers the insulation sizing and mass calculations, and Sec II.B covers the thermal and resistance modeling. Lastly Sec II.C details the formulation of the optimization problem. In Sec III, results and discussion are presented, which show the effect of differences in the cable model approaches for the selected mission. Conclusions are presented in Sec IV

II. Methodology

The cable model is broken into two parts: insulation and mass calculations, and thermal and resistance calculations. Both insulation and mass are time-invariant values that won't change during the mission. These calculations will be covered in Sec II.A. Thermal and resistance values do vary over the mission duration, unless specific steady-state assumptions are made. These calculations will be covered in Sec II.B. Lastly, the cable subsystem optimization mission formulation is described in Sec II.C. This last section covers the 6-passenger Urban Air Mobility (UAM) mission outputs that will be used as inputs to the cable optimizations.

A. Insulation and Mass

Here, equations are presented to compute time-invariant quantities such as insulation thickness and mass-per-length based on the general form shown in Eq. 1 & 2. In this section these equations will be fully developed into analytic expressions.

$$t_i = f\left(\epsilon, V_{max}, t_v, \alpha, r_c\right) \tag{1}$$

$$\bar{m}_{tot} = f\left(t_i, r_c, \rho_i, t_s, \rho_s\right) \tag{2}$$

Insulation thickness is computed using the SVD method described by Cheng[9] via Eq. 3 and Eq. 4. These methods do not depend on conductor material and it is assumed that they are valid for both copper and aluminum conductors.

$$t_i = r_c * \left(\exp(\frac{K \cdot V_{max} \cdot t_v}{\alpha \cdot r_c}) - 1 \right) + C \tag{3}$$

$$K = \frac{3\epsilon}{1 + 2\epsilon} \tag{4}$$

t_i is the insulator thickness, r_c is the radius of the conductor, K is the shape factor of the void which is assumed to be spherical, V_{max} is the maximum voltage of the line during the mission, t_v is the thickness of the void or inclusion which is assumed to be $0.0050cm$,[9,14] and α is the minimum breakdown voltage of air in the cavity which is assumed to be $340V$.[15] C is a constant with a value of $0cm$ for cables with voltages at or above $20kV$ and $0.1cm$ for cables with lower voltage. This factor allows better matching between actual cables and the empirical formula for low-voltage cables.[9] Lastly, ϵ is the dielectric permittivity of the material. An illustration of the cable using this nomenclature is shown in Fig. 2.

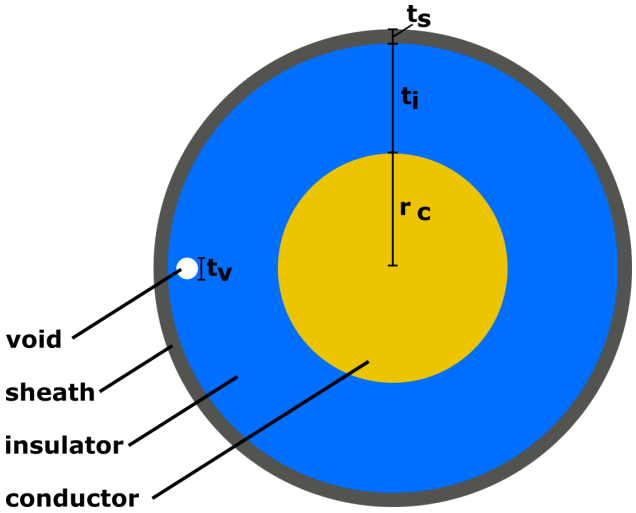

Figure 2: Cross-section view of cable.

Eq. 3 produces an insulation thickness that exceeds International Electrotechnical Commission (IEC) 502 standards for $10kV$ and $20kV$ cables.[16] This is because the maximum voltage can be derated with the assumption that electrical discharges on the order of $2pC$ are innocuous[17]. The derated voltage is found by multiplying V_{max} by $\sqrt{2/3}$. Adding this factor into Eq. 3 yields our final thickness estimate:

$$t_i = r_c * \left(\exp(\frac{K \cdot V_{max} \cdot \sqrt{2/3} \cdot t_v}{\alpha \cdot r_c}) - 1 \right) + C \tag{5}$$

It is now easy to show how Eq. 5 can reproduce similar outputs to the IEC 502 standards. In Table 1 comparisons are included for 10kV and 20kV cables insulated with polyvinyl chloride (PVC). These results match well with Cheng[9] and were created with the assumption that ϵ is 8 for PVC at $50Hz$ and 90^OC.[18]

Table 1: Cable insulation results and verification assuming PVC insulation

$V_{max}(V)$	$r_c(cm)$	$C(cm)$	ϵ	K	$t_v(cm)$	Eq. 5, $t_i(cm)$	IEC, $t_i(cm)$
10000	0.24	0.1	8	1.4	0.005	0.34	0.40
15000	0.30	0.1	8	1.4	0.005	0.51	0.52
20000	0.35	0.0	8	1.4	0.005	0.57	0.57

Cable mass-per-length can now be calculated as the summation of conductor, insulator, and sheath mass. Conductor mass-per-length $\bar{m}_c$ is calculated by determining the conductor area, A_c, and multiplying by the conductor density ρ_c as follows:

$$A_c = r_c^2 \cdot \pi \tag{6}$$

$$\bar{m}_c = A_c \cdot \rho_c \tag{7}$$

Insulator mass-per-length, $\bar{m}_i$, is calculated by finding A_i, which is the area of the insulator and multiplying by ρ which is the density of the insulation material.

$$A_i = (t_i + r_c)^2 \cdot \pi - r_c^2 \cdot \pi \tag{8}$$

This reduces to:

$$A_i = \left(t_i^2 + 2 \cdot t_i \cdot r_c\right) \cdot \pi \tag{9}$$

$$\bar{m}_i = A_i \cdot \rho_i \tag{10}$$

Similarly, the sheath area is determined by assuming a sheath thickness, t_s, which is typically on the order of $0.1cm$.

$$A_s = (t_s + t_i + r_c)^2 \cdot \pi - (t_i + r_c)^2 \cdot \pi \tag{11}$$

EQ. 11 reduces to:

$$A_s = \left(t_s^2 + 2 \cdot t_s \cdot t_i + 2 \cdot t_s \cdot r_c\right) \cdot \pi \tag{12}$$

The sheath mass-per-length, $\bar{m}_s$, is a function of the sheath material density, ρ_s, and can now be calculated:

$$\bar{m}_s = A_s \cdot \rho_s \tag{13}$$

Finally, cable mass-per-length is the summation of conductor mass-per-length, $\bar{m}_c$, insulator weight, $\bar{m}_i$, and sheath weight, $\bar{m}_s$, thus:

$$\bar{m}_{tot} = \bar{m}_c + \bar{m}_i + \bar{m}_s \tag{14}$$

B. Thermal and Resistance

This section describes calculations for the thermal state of the conductor and insulator as well as the conductor resistance. The thermal method presented is based on a first order lumped capacitance modeling approach, and holds valid for Biot numbers less than 0.1.[19] A simplified model of the cable is used to track temperatures. This model has two states: the temperature of the conductor, T_c, and the insulator, T_i,. These are later combined into a single conductor and insulator temperature, T_{ci}. As a simplification, the sheath thickness is added to the insulator thickness and the material properties are assumed to be similar. A separate sheath analysis could be easily created using the equations provided and would allow the sheath to have different material properties than the insulator. Heat generated in the conductor, Q_c, is propagated to the insulator via conduction. The electrical resistance of the cable fluctuates as a function of conductor temperature. The cable, which is suspended in the wing box, transfers heat to the ambient air through free convection. This configuration is shown in Fig. 3.

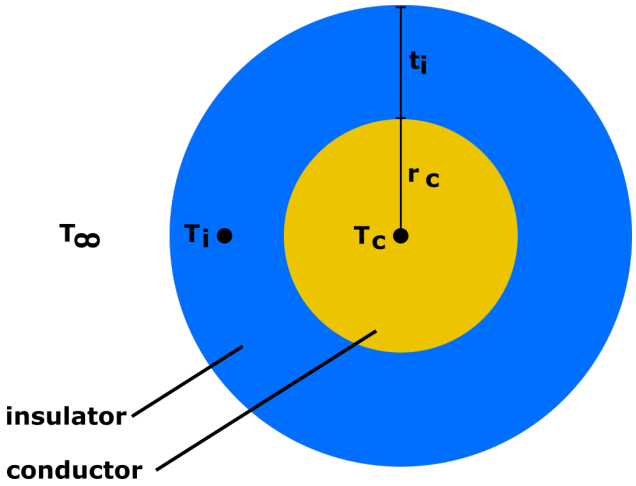

Figure 3: Simplified thermal model of cable

The general form of the ordinary differential equations describing how the temperatures of the cable components change in time are shown in Eq. 15 and Eq. 16.

$$\frac{dT_c}{dt} = f\left(I, R_c, r_c, k, T_c, T_i, t_i, CP_c, \rho_c\right) \tag{15}$$

$$\frac{dT_i}{dt} = f\left(r_i, k, T_c, T_i, t_i, h, T_\infty, CP_i, \rho_i, r_c\right) \tag{16}$$

These functions are built from the basic convection and conduction heat transfer concepts:

$$\frac{dT_c}{dt} = \frac{Q_c - Q_i}{HC_c} \tag{17}$$

$$\frac{dT_i}{dt} = \frac{Q_i - Q_\infty}{HC_i} \tag{18}$$

T_c and T_i are the temperature states of the cable and insulator, t is time and d/dt is a time derivative operator, Q is the heat input or output, HC is the heat capacity of the cable or insulator. Heat capacity per-length is used so that the cable length does not need to be an input to the calculations.

$$HC = CP \cdot \rho \cdot A \tag{19}$$

CP is the specific heat of the material, ρ is the density of the material, and A is the cross-sectional area of the material. While CP does change as a function of temperature, this change is relatively small for the temperature range examined. CP_c for the copper conductor is assumed to be $386 J/kg/C$.[20] When using an aluminum conductor, a CP_c of $902 J/kg/C$ is assumed.[20] CP_i depends on the insulator material. Substituting the calculations for A, which was provided in Eq. 6 and 9, yields the following:

$$HC_c = CP_c \cdot \rho_c \cdot r_c^2 \cdot \pi \tag{20}$$

$$HC_i = CP_i \cdot \rho_i \cdot (t_i^2 + 2 \cdot t_i \cdot r_c) \cdot \pi \tag{21}$$

Now the heat generated or lost from each component can be calculated as follows:

$$Q_c = I^2 \cdot R_c \tag{22}$$

$$Q_i = C_c \cdot k \cdot \frac{T_c - T_i}{t_i} \tag{23}$$

$$Q_\infty = C_i \cdot h \cdot (T_i - T_\infty) \tag{24}$$

I is the current flowing through the cable, R_c is the conductor resistance-per-length, k is the thermal conductivity of the insulator, h is the convective heat transfer coefficient, C_c is the circumference of the conductor, C_i is the outer circumference of the insulator, and T_∞ is the temperature of the ambient air inside the wing box. Substituting out circumference in Eq.s 23, 24, in favor of radius yields the following equations:

$$Q_i = 2 \cdot r_c \cdot \pi \cdot k \cdot \frac{T_c - T_i}{t_i} \tag{25}$$

$$Q_\infty = 2 \cdot (t_i + r_c) \cdot \pi \cdot h \cdot (T_i - T_\infty) \tag{26}$$

With the expressions for Q (Eq. 22, 25, 26) and HC (Eq. 20, 21), all the pieces are available to construct an OpenMDAO group that calculates $\frac{dT_c}{dt}$ and $\frac{dT_i}{dt}$ (Eq. 17, 18). Preliminary simulations indicated tracking two temperatures captured second order effects compared to tracking a single combined cable and insulator temperature, T_{ci}. However, because the difference between results was small and because it is easier to implement single temperature tracking, the remaining analysis in the paper will only cover the combined cable temperature case. To assemble a single differential equation for $\frac{dT_{ci}}{dt}$, the change in the combined temperature over time, Eq. 17 and 18 can be combined as follows:

$$\frac{dT_{ci}}{dt} = \frac{Q_c - Q_\infty}{HC_c + HC_i} \tag{27}$$

The steady-state temperature of the combined cable can be found by setting $\frac{dT_{ci}}{dt}$ to zero, which means $Q_c - Q_\infty$ must also be zero. Substituting in Eq. 26, and Eq. 22 yields:

$$Q_c - Q_\infty = 0 = I^2 \cdot R_c - (2 \cdot (t_i + r_c) \cdot \pi \cdot h \cdot (T_i - T_\infty)) \tag{28}$$

Assuming that T_i is equivalent to T_{ci} we can rearrange to solve for T_{ci} directly:

$$T_{ci} = \frac{I^2 \cdot R_c}{2 \cdot (t_i + r_c) \cdot \pi \cdot h} + T_\infty \tag{29}$$

The steady-state temperature estimate will typically be larger than temperatures from a transient analysis. This causes steady-state optimizations to carry extra margin as will be shown in Sec III.

Conductor resistance can be calculated based on the conductor material and the conductor temperature as follows:

$$R_c = R_{ref} * (1 + \alpha_r(T_c - T_{ref})) \tag{30}$$

R_c is the resistance of the conductor, R_{ref} is the resistance at the reference temperature (typically $20^O C$), α_r is the resistance temperature scale factor, T_c is the conductor temperature, and T_{ref} is the temperature where the reference resistance was calculated. Both copper and aluminum conductors were examined in this work. The α_r values for copper and aluminum were assumed to be 0.00393 (1/C) and 0.004308 (1/C) respectively. For steady-state optimizations, this resistance is considered fixed at the maximum continuous rated temperature of the cable ($T_c = 90^O C$). This avoids having to create a solver in the steady-state optimization to feed the calculated temperature value back into the resistance calculations. This will simplify the coupling in the model, but it will cause the cable to heat up slightly faster as a result of assuming the worst case resistance. For transient optimizations, the resistance is allowed to change based on the current temperature of the cable ($T_c = T_{ci}$). T_{ci} is found by integrating Eq. 27 over time. This approach takes full advantage of Eq. 30 because T_c when the cable temperature is lower during most of the mission, the associated lower resistance will reduce the heat produced. This results in significantly less heat created from resistance during the mission.

For validation, published cable temperatures can be compared against temperatures calculated using steady-state analysis from Eq. 29 and transient analysis run to steady-state from Eq. 27. For this example a pure copper Gexol marine power distribution cable[21] with a V_{max} of 2000V is used. The ambient temperature, T_∞, is assumed to be $30^O C$. The Gexol insulation is assumed to have a density, ρ_i, of $1.45 g/cm^3$ and a DC dielectric permitivity , ϵ, of 4.0. The insulation material is assumed to be compatible with both copper and aluminum conductors. CP_i is assumed to be $2800 J/kg/C$ and the sheath thickness,t_s, is assumed to be $0.06 cm$ for 10 American Wire Gauge (AWG) and $0.12 cm$ for all the other cables. Cable resistance values were calculated using Eq. 30 at the reference temperatures listed in Table 2. The convective heat transfer coefficient, h, was tuned to a value of $0.0011 W/cm^2/C$ to best match published data.[21] Parameter tuning helped to account for differences in the model which assumes a solid cable vs. the Gexol cable which is stranded. The tests results for the steady-state and transient analysis match closely with the published data and are presented in Table 2.

Table 2: Cable thermal and weight estimation from transient and steady-state models via Eq. 27 & 29

AWG	Conductor Radius (cm)	Ampacity (A)	Ref Temp (C)	Transient Temp (C)	Steady State Temp (C)	Ref $\bar{m}_{tot}$ (kg/m)	Calc $\bar{m}_{tot}$ (kg/m)
10	0.129	50	75	77	77	0.086	0.088
10	-	55	90	89	89	-	-
8	0.1632	70	75	75	74	0.140	0.143
8	-	80	90	92	92	-	-
6	0.2057	95	75	78	77	0.1949	0.196
6	-	105	90	90	91	-	-
4	0.2595	125	75	76	76	0.2694	0.279
4	-	140	90	90	91	-	-

C. Optimization Formulation

A cable sub-optimization can now be constructed using the equations developed in Sec II.A and Sec II.B and input parameters from an optimized 6-passenger quadrotor mission. This is considered a sub-optimization because the whole 6-passenger vehicle is not being re-optimized based on the outputs of the cable analysis. The mission involves flying the 6-passenger quadrotor a distance of 70km, with vertical takeoff and landing maneuvers at the start and end of the mission. The altitude profile, motor power demand, and battery voltage are all similar to previously published missions.[3,5] The cables carry electricity directly from the battery to the motors. As the battery discharges during the mission, the voltage drop across the cables decreases.[3,5] This effect combined with constant motor power demands through the majority of the flight causes the individual cables to have the current profile shown in Fig. 4a.

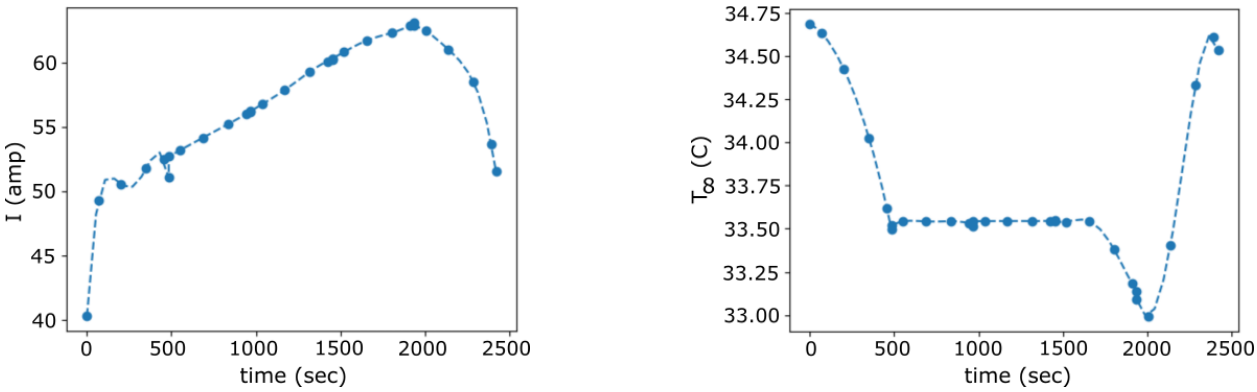

(a) Cable amperage during the mission

(b) Temperature inside the wingbox during the mission

Figure 4: Optimization mission inputs

Both steady-state and transient optimizations are analyzed. Steady-state optimizations use a fixed amperage demand of 63.06 amps, which corresponds to peak amperage during the flight. Steady-state ambient temperature is be fixed at $34.7^{O}C$, which includes a $10^{O}C$ increase from standard atmosphere temperature to provide a little temperature margin . This factor helps account for the lack of air circulation inside the wingbox. The maximum voltage during the mission, V_{max}, is $720V$ and the total cable length is the same as the 6-passenger model (88 meters). The sheath thickness t_s for the cables is assumed to be fixed at $0.12cm$. This will cause some additional inaccuracies for small cables making them appear cooler and slightly heavier. However the accuracy of the larger cables (8-4AWG), which are more relevant for this study, will be maintained. Lastly, steady-state analysis will assume a fixed resistance at the maximum continuous operating temperature of the cable ($90^{O}C$). Inputs for the transient optimization include the T_∞ thermal profile for ambient temperature and the amperage profile for the motors which are shown in Fig. 4. The air inside the wing box, including the $10^{O}C$ off-set from ambient, is shown in Fig. 4b. Resistance is also allowed to vary as a function of cable temperature, T_{ci}.

The optimization seeks to minimize total cable mass subject to a $90^{O}C$ constraint on cable temperature. The steady-state optimization assumes a constant cable temperature for the whole mission, whereas the transient optimization assumes a time-varying cable temperature. Separate optimizations were run to vary the number of parallel cables. The number of parallel cables is a discrete quantity and it is useful to determine if a single large cable is more effective than multiple smaller cables. The optimizer will be allowed to vary the inputs shown in Table 3. The material percentage assumes it is possible to make a cable out of some percentage of aluminum and copper. While this is not necessarily practical, it allows the optimizer to demonstrate a preference for a conductor material. The formulation is continuous and adjusts the conductor density (ρ_c), resistance (R_c), and specific heat (CP_c) accordingly.

III. Results and Discussion

Results from optimizing the cable models in Sec II.A and Sec II.B using the input profiles from Sec II.C are presented next. A discussion follows to analyze the results and highlight the applicability to future UAM studies.

Table 3: Optimization Design Variables, States, Constraints

	Type	Lower Bound	Upper Bound
Conductor Radius (r_c)	Design Variable	0.1 (cm)	0.3 (cm)
Material Percentage	Design Variable	0 (Aluminum)	100 (Copper)
Cable Temperature (T_{ci})	State	-	90 (^OC)

A. Optimization Results

The results from eight different optimizations are shown in Table 4. Three different design methods are shown in the table: COTS, steady-state, and transient. As a reminder, the COTS design methods selects a cable based on maximum amperage draw during the mission. Steady-state design also uses the max mission amperage with the addition that the insulation thickness can be adjusted based on the max mission voltage. Lastly, the transient method designs cables based on their performance throughout the mission while considering thermal effects on the order of minutes. The optimization goal was to minimize cable mass. The initial condition for cable material was 100% copper. The total run-length of cable is 88 meters and is the same in each test case. The number of parallel runs of cable was set to one for all these results.

Table 4: Cable mass and temperature results by design method and *temperature constraint.

Design Method	Optimization Method	Copper (%) (0 = Al)	Radius (cm) Conductor	Max Temp (C) Estimated (Eq. 29)	Max Temp (C) Mission Max (Eq. 27)	Mass (kg)
COTS	None	100	0.163	73	67	12.55
-	None	0	0.2057	68	62	9.96
Steady State	Radius	100	0.143	90*	85	9.92
-	Material	32	0.163	90*	85	8.68
-	Combined	0	0.172	90*	85	7.54
Transient	Radius	100	0.138	95	90*	9.50
-	Material	10	0.163	95	90*	7.66
-	Combined	0	0.166	95	90*	7.29

For the COTS method, a copper 8AWG Gexol cable and an aluminum 6AWG cable were selected based on their ability to handle the peak amperage during the mission. Due to a lack of published data on an aluminum cable variant, the aluminum COTS cable is based on a 6AWG Gexol copper cable with a derated ampacity. Since these cables were not modified, the optimization column inTable 4 lists 'None'. These cables resulted in the heaviest mass. Attempts to use smaller cables would have exceeded their rated amperage. Steady-state simulations estimate the maximum temperature for the copper cable to be 73^OC, but the transient analysis showed that the cable experienced a maximum of only 67^OC. Similarly, the COTS aluminum variant only experienced temperatures of 68^OC in steady-state and as little as 62^OC with transient analysis. The mission temperature results indicate that the cable is over-designed for this particular vehicle and mission. The margin on cable temperature is achieved due to large conductor and insulator mass. These cables have more insulation because they are designed to 2000V as opposed to the rest of the non-COTS cables designed for only 720V. In the other optimizations, it is evident that as temperature margin shrinks, the mass also decreases.

The steady-state design method cases are shown next. There are three different optimization criteria used for this method including optimizing only conductor radius, optimizing only the conductor material, and a combined optimization of material and radius. Each of these methods gives the optimizer different design variables to reduce weight and they are successful at this when compared with the COTS method. Steady-state design only uses information gained in the steady-state analysis to perform the optimization. Thus, the constraints for these designs are placed on the steady-state temperature results. All three optimization methods result in a steady-state cable temperature of 90^OC, which is the maximum allowed continuous operating temperature. The steady-state radius optimization reduces conductor radius and has a reduced cable insulation thickness compared to the COTS copper cable. The radius optimized cable has 21% less weight than the equivalent COTS option. The steady-state material optimization manages to reduce copper

percentage to 32% before hitting the temperature constraints. The resulting cable is partially copper and partially aluminum, which may not be possible in a metallurgical sense. However this does demonstrate the preference of the optimizer to move away from copper conductors to decrease mass. The combined optimization produces better results than the material or radius optimization individually, showing that its important to consider both degrees of freedom to get the best overall performance. Examining the results from the actual temperatures experienced during the mission, it can be seen that the mission temperatures are slightly lower than the steady-state estimates. From an optimization standpoint, this indicates the cable is still over-designed and the margin could be reduced further with a transient analysis.

The transient design method also explores radius, material, and combined optimizations. In these cases, the cable temperature constraint of $90^{O}C$ was placed on the maximum cable temperature calculated during the mission. The transient cable radius optimization hits the maximum temperature but does it by decreasing cable radius. Comparing this result with the COTS copper cable, demonstrates a mass reduction of 24%. The material optimization is able to reduce the copper percentage to only 10% before reaching a mission max temperature of $90^{O}C$. Finally, the combined transient optimization of material and radius shows the lightest cable weight of all the optimizations. This cable is 100% aluminum. A comparison against the COTS aluminum cable shows a 27% reduction in cable mass. The steady-state temperature analysis of the cable shows that it should reach $95^{O}C$ if it were run continuously at peak amperage. However, the transient analysis shows that the maximum temperature reached during the mission is only $90^{O}C$. The cable thermal profile for this case is shown in Fig. 5a.

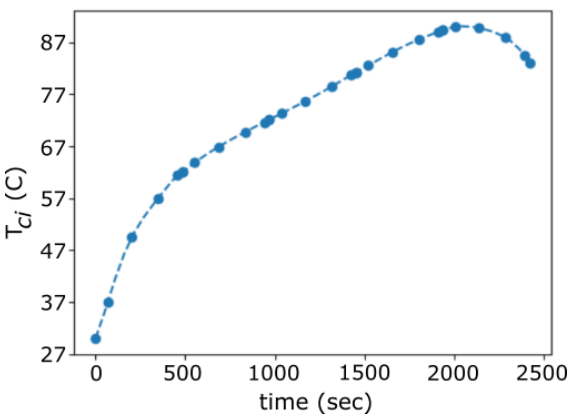

(a) T_{ci} Cable Thermal Profile, 1-Parallel Run, Transient Combined Optimization

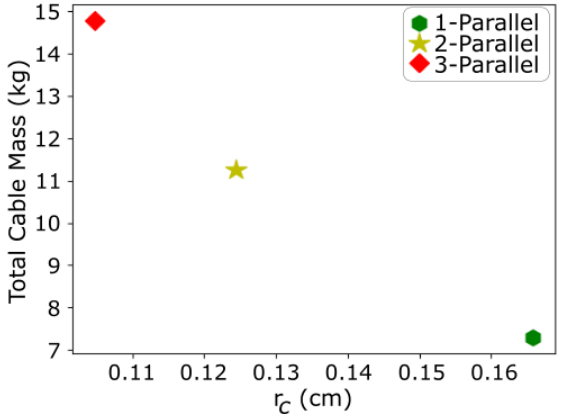

(b) Comparison of Number of Parallel Cable Runs, Transient Combined Optimization,

Figure 5: Cable Subsystem Optimization Results

B. Discussion

The methods shown in this paper demonstrate how to build optimizations that can smoothly explore trade-offs between cable thickness and material composition while considering thermal and power constraints. These models are useful in eVTOL conceptual level design studies where the best overall performance is achieved by balancing the competing performance of all sub-systems. The continuous solution space allows gradient based optimization to be applied cable subsystem design, which gives fast performance even when considering transient models. The comparison between the COTS cable, the steady-state optimization, and the transient optimization demonstrates the effects of problem formulation on cable mass and temperature margin. In the COTS cases, the cables are heavy and this weight is due to the large temperature margin and there is excess insulation. The COTS cables are designed expecting a maximum voltage of 2000V but the vehicle only runs at 720V maximum. The steady-state combined optimization shows that using a lower voltage allows cable results in a lighter cable. The transient combined analysis gives the lightest design by exploiting the relatively narrow temperature peak of the mission to keep the cable at its absolute smallest possible size. Even with this final design, there is still margin in the cable design. This is because the mission max temperature constraint was based on the maximum continuous operating temperature for the cable. Therefore, excursions from this temperature for short amount of time would be acceptable. Thus while the

cable was optimized for a particular mission, it is capable of supporting a variety of UAM mission profiles. One potential addition to the mission profile would be an emergency 2 minute hover at the end of the cruise mission. It is intuitive that this would cause a final temperature spike, but the the temperature at the end of cruise has already fallen far enough from its peak that this is not likely to result in a limiting condition for this aircraft. None the less, in a detailed analysis adding additional mission segments, such as a 2 minute hover at the end of the cruise, could be considered.

By using a custom designed cable, the best designs offered a 5.3kg reduction compared to a copper COTS and 2.67kg reduction compared to a notional aluminum COTS cable. In reality, the manufacturer of the COTS option considered in this work does not offer an aluminum COTS design. Therefore only the 5.3kg reduction compared to a copper COTS cable will be considered further. In keeping with the constant gross weight assumption, the mass decrease of 5.3kg from the copper COTS configuration to the transient combined configuration represents an additional 5.3kg of payload the aircraft could carry. Since the gross weight stayed the same, the overall energy usage for the aircraft would be constant as well. Future work could consider a more complete aircraft design process where the whole aircraft would be resized to account for the reduction in empty weight, which would provide a way to link reduced cable weight to overall energy usage. While 5.3kg mass reduction may seem small, it is important to note that these results were for a 6-passenger UAM with just 88 meters of cable. Large aircraft with longer cables and larger power demand may see an increased effect.

Transient designs should give decreased mass compared to steady-state designs because in any situation where the mission doesn't provide an steady-state condition that is thermally limiting. EAP systems do not necessarily reach steady-state conditions during their short missions, due to the lack of any prolonged constant current or constant temperature mission segments.

Although the transient design approach does yield lower weight, the savings over the steady-state design was less than 1 kg because the mission transients were not severe enough to cause a larger difference. The transient design approach is more complex as well, so there is a trade-off between modeling complexity and mass savings. The steady-state design is easier to implement, but the transient design yields better results. However, the combined cable temperature equations used by both of these methods slightly underestimate conductor resistance, which changes as a function of temperature. The modeling complexity and accuracy could be further enhanced by tracking these temperatures separately and connecting conductor temperature to the conductor resistance. This could be done both in steady-state analysis and transient analysis and would require the use of additional solvers, further increasing modeling complexity. Which design method is best for a particular vehicle model will depend on how much effort a project can spend on implementing the cable model, and how significant mass-reduction in this subsystem could be on the rest of the vehicle.

For all of the optimizations studied, a single large cable was found to be more mass-efficient than having two or even three parallel cable runs. The comparison of multiple parallel cables for the transient combined optimization is shown in Fig. 5b. Similar results were seen from the steady-state combined optimization. None of these studies could support the assumption that weight could be reduced by increasing the number of parallel cables. This analysis supports the assertion that mass reduction due to multiple cable runs only happens when using COTS cables with fixed conductor diameters, which create step functions in the solution space. Furthermore, even when accounting for single-fault redundancy by adding an extra cable run, the optimal solution was still to use the smallest number of large cables. There may be physical bend radius constraints that may prevent such a cable from actually being used on the aircraft. This type of constraint could be implemented as an upper bound on conductor radius and may directly affect the optimal number of parallel cables.

The methods presented in this paper provide a guideline on how alternative cable material and insulation configurations can be evaluated. In each of the optimizations, aluminum was selected as the cable material by the optimizer over copper when it was permitted. If there were constraints on cable volume, these results may have been different. However, this does shows the ability of the optimizer to help guide material selection. Any other conductor material could have been substituted for aluminum and evaluated against the basic copper cable. Depending on the assumptions provided for that material and the optimization, it is possible to observe a preference for one material over another.

IV. Conclusion

Due to the nature of designing novel Electrified Aircraft Propulsion (EAP) vehicles, it is important to consider new power cable design approaches that account for the time-varying power and thermal profiles in order to enable lower weight power transmission systems. The methods presented in this paper accomplish this by creating a continuous solution space that a gradient-based optimizer can explore. This is valuable when studying the trade-offs and interactions between EAP subsystems. This work examined three different design processes applied to a 6-passenger Urban Air Mobility (UAM) aircraft with a prescribed power profile: selection of a commercial off-the-shelf (COTS) cable, a custom cable designed with steady-state assumptions, and a custom cable designed with transient assumptions. Steady-state optimization was effective at reducing cable mass by up to 24% when compared with copper COTS cables. Transient optimization was able to further reduce cable mass by a small amount. This could have been more significant if there were larger variations in the current demand and ambient temperature during the mission. While the transient model did produce the best results, it was more complex to implement compared to the steady-state model. Material optimizations consistently demonstrated preference for aluminum over copper cables. Lastly, it was more effective to select a single large cable vs. multiple smaller cables. The methods presented can be applied during the conceptual design of UAM concepts to estimate power cable mass. They also present a means of considering conductor material selection (e.g. aluminum vs. copper) for power cable design in the context of overall aircraft performance.

The data presented shows that the simplified physics used in this work can reproduce the mass for COTS cables accurately using a steady-state modeling approach. This result validates the general modeling method for computing insulation thickness and overall cable temperature. The models, having been shown to be able to replicate the COTS results, were then used to size a custom cable for a specific aircraft using both steady-state and transient design methods. The results showed that the 6 passenger UAM aircraft could reduce the power cable weight by 5.3kg using a custom cable compared to a copper COTS cable and 2.67kg savings compared to a notional aluminum COTS cable. Roughly half the overall weight savings was due to using the lighter material, and half due to using a custom designed cable based on the specific aircraft mission requirements. However, it is important to reiterate that the none of the sizing presented for the COTS or custom designed cables accounted for all of the guidelines included in SAE-AS50881[8] which would be required for a detailed cable design. For conceptual system studies, a simple multiplier on the computed cable mass (e.g. 1.2) should be sufficient to account for expected design margins. Although the specific value of that multiplier should be chosen with some care. Future work in this area may consider more direct ways to integrate design safety margins into the analysis, such as considerations of local hot spots in the insulation, accounting for for worst case mission scenarios, or additional uncertainty quantification to account for variation in operating conditions.

Acknowledgements

The work presented in this paper is supported by NASA's Transformational Tools and Technologies (TTT) Project. This work was performed in collaboration with Electrical Modeling and Thermal Analysis Toolbox (EMTAT), which is developing Matlab-based tools for electric aircraft propulsion.[13]

References

[1]Schnulo, S. L., Chapman, J. W., Hanlon, P., Hasseeb, H., Jansen, R., Sadey, D., Sozer, E., Jensen, J., Maldonado, D., Bhamidapati, K., Heersema, N., Antcliff, K., Frederick, Z. J., and Kirk, J., "Assessment of the Impact of an Advanced Power System on a Turboelectric Single-Aisle Concept Aircraft," *AIAA Propulsion and Energy 2020 Forum*.

[2]Aretskin-Hariton, E., Schnulo, S., Hendricks, E., and Chapman, J., "Electrical Cable Design for Urban Air Mobility," *AIAA Scitech 2020 Forum*, Orlando, FL, 2020.

[3]Hendricks, E. S., Hariton, E., Ingraham, D., Gray, J. S., Schnulo, S. L., Chin, J., Falck, R., and Hall, D., "Multidisciplinary Optimization of an Electric Quadrotor Urban Air Mobility Aircraft," *AIAA Aviation 2020 forum*, Reno, NV, 2020.

[4]Chapman, J. and Schnulo, S., "Development of a Thermal Managment System for Electrified Aircraft," *2020 AIAA SciTech Forum*, January 2020.

[5]Chin, J., Aretskin-Hariton, E., Ingraham, D., Hall, D., Schnulo, S., Gray, J., and Hendricks, E., "Battery Evaluation Profiles for X-57 and Future Urban Electric Aircraft," August 2020.

[6]Johnson, W., Silva, C., and Solis, E., "Concept Vehicles for VTOL Air Taxi Operations," *HS Technical Conference on Aeromechanics Design for Transformative Vertical Flight*, San Francisco, January 2018.

[7]Silva, C., Johnson, W., Solis, E., Patterson, M., and Antcliff, K., "VTOL Urban Air Mobility Concept Vehicles for Technology Development," *American Institute of Aeronautics and Astronautics*, June 2018.

[8]*AS50881: Wiring, Aerospace Vehicle*, SAE International, 2019.

[9]Cheng, F. C., "Insulation thickness determination of polymeric power cables," *IEEE Transactions on Dielectrics and Electrical Insulation*, Vol. 1, No. 4, 1994, pp. 624–629.

[10]Vratny, P. C., "Conceptual Design Methods of Electric Power Architectures for Hybrid Energy Aircraft," *Masters Thesis, Technischen Universität München*, 2018.

[11]Gray, J. S., Hwang, J. T., Martins, J. R. R. A., Moore, K. T., and Naylor, B. A., "OpenMDAO: An Open-Source Framework for Multidisciplinary Design, Analysis, and Optimization," *Structural and Multidisciplinary Optimization*, Vol. 59, 2019, pp. 1075–1104.

[12]Falck, R. D. and Gray, J. S., "Optimal Control within the Context of Multidisciplinary Design, Analysis, and Optimization," *AIAA Scitech 2019 Forum*, AIAA, San Diego, CA, 2019.

[13]Bell, M. E. and Litt, J. S., "An Electrical Modeling and Thermal Analysis Toolbox for Electrified Aircraft Propulsion Simulation," *AIAA Propulsion and Energy 2020 Forum*, New Orleans, LA, 2020.

[14]Cheo, P. K., Luther, R., and Porter, J. W., "Detection of Voids and Contaminants in Polyethylene Insulated Cable Utilizing a Fir Laser Beam," *IEEE Transactions on Power Apparatus and Systems*, Vol. PAS-102, No. 3, 1983, pp. 521–526.

[15]Dakin, T. W., Luxa, G., Operman, G., Vigreux, J., Wind, G., and Winkelnkemper, H., "Breakdown of Gases in Uniform Fields Paschen Curves for Nitrogen, Air and Sulfur Hexafluoride," *Electra*, Vol. 32, 1974, pp. 61–82.

[16]Commission, I. E., "IEC Standard, Publication 502: Extruded Solid Dielectric Insulated Power Cables for Rated Voltages from 1kV to 30kV," *IEC Central Bureau, Geneva*, Vol. 3rd Edition, 1983 Amendment 2, 1987. Amendment 3, 1989.

[17]Howard, P. R., "The Effect of Electric Stress on the Life of Cables Incorporating a Polythene Dielectric," *Proceedings IEE*, Vol. 98, 1951, pp. 365–370.

[18]Orrit-Prat, J., Mujal-Rosas, R., Rahhali, A., Marin-Genesca, M., Colom-Fajula, X., and Belana-Punseti, J., "Dielectric and mechanical characterization of PVC composites with ground tire rubber," *Journal of Composite Materials*, Vol. 45, No. 11, 2011, pp. 1233–1243.

[19]Bergman, T. L., Lavine, A. S., Incropera, F. P., and DeWitt, D. P., *Fundamentals of Heat and Mass Transfer*, John Wiley Sons, Inc., Hoboken, New Jersey, 7th ed., 2011.

[20]Jensen, J. E., Tuttle, W. A., Stewart, R. B., Brechna, H., and Prodell, A. G., "Selected Cryogenic Data Notebook," *Brookhaven National Laboratory, BNL-10200-R*, Vol. 1, Sections 8, August 1980.

[21]"Downstream Power, Control & Instrumentation Cables," *Nexans AmerCable Incorporated*, Katy, Taxas, 2019.